Arch. Pharm. Res. (2021) 44:182–193
https://doi.org/10.1007/s12272-020-01264-9

Online ISSN 1976-3786
Print ISSN 0253-6269

Archives of Pharmacal Research
www.springer.com/12272

RESEARCH ARTICLE

Hyperthermal paclitaxel-bound albumin nanoparticles co-loaded with indocyanine green and hyaluronidase for treating pancreatic cancers

Sung Soo Kim[1] · Hwang Kyung Kim[1] · Hanju Kim[1] · Woo Tak Lee[1] · Eun Seong Lee[2] · Kyung Taek Oh[3] · Han-Gon Choi[4] · Yu Seok Youn[1]

Received: 15 July 2020 / Accepted: 11 August 2020 / Published online: 17 August 2020

Abstract Albumin nanoparticles have become an attractive cancer nanomedicine platform due to their pharmaceutical advantages. Recently, photothermal therapy has been extensively applied to cancer treatment due to heat-induced tumor ablation. Herein, we fabricated albumin nanoparticles (HSA-NPs) loaded with paclitaxel (PTX), indocyanine green (ICG; a hyperthermal agent) and hyaluronidase (HAase) that breaks down hyaluronan, a major component of the extracellular matrix (ECM) in tumors. Synthesis was based on a slightly modified nanoparticle albumin-bound (Nab™) technique. The prepared nanoparticles (PTX/ICG/HAase-HSA-NPs) had a spherical shape with an average size of ~ 110 nm and a zeta potential of ~ -30.4 mV. They displayed good colloidal stability and typical patterns of ICG, HSA and HAase in UV–VIS–NIR and circular dichroism spectroscopic analysis. PTX/ICG/HAase-HSA-NPs were found to have excellent hyperthermal effects in response to near-infrared laser irradiation (808 nm) (up to > 50 °C over 4 min). The hyperthermia conducted by PTX/ICG/HAase-HSA-NPs resulted in significant cytotoxicity to pancreatic AsPC-1 cells at both severe (> 50 °C) and mild (41–42 °C) hyperthermal states in conjunction with the inherent cytotoxic activity of paclitaxel. Furthermore, the confocal images of AsPC-1 cell spheroids proved PTX/ICG/HAase-HSA-NPs were able to permeate deeply into the three-dimensional tumor tissue mimicry structure. Most of all, PTX/ICG/HAase-HSA-NPs maintained all these physicochemical and anti-cancer properties irrespective of the amount of embedded HAase (1–5 mg). Our results demonstrated that PTX/ICG/HAase-HSA-NPs are a promising hyperthermal/chemotherapeutic anticancer agent.

Keywords Indocyanine green · Hyaluronidase · Hyperthermal therapy · Albumin nanoparticles · Tumor targeting

Introduction

Albumin has been viewed as one of the most useful natural materials in developing anticancer nanomedicines (Kratz 2008, 2014; Lee and Youn 2016). It is biodegradable, biocompatible, highly soluble in aqueous media, chemically stable and resists the glomerular filtration that shortens the circulation half-lives of drugs/carriers (Kratz 2008; Thao et al. 2016). Moreover, it is a highly effective targeting carrier for tumors. Actually, albumin or nanoparticles made of albumin are well known to accumulate in tumors through both passive tumor extravasation and active gp60-mediated transcytosis (Bae et al. 2012; Lamichhane and Lee 2020). There have been a large number of applications of albumin nanoparticles for this purpose, as well as a variety of fabrication methods. Among these, the Nab™ (nanoparticle albumin-bound)-based formulation is an excellent example. Its paclitaxel (PTX) product, Abraxane® (Celgene Corp.), has rapidly replaced the clinical market of Taxol® due to

✉ Yu Seok Youn
ysyoun@skku.edu

1 School of Pharmacy, Sungkyunkwan University, 2066 Seobu-ro, Jangan-gu, Suwon 16419, Gyeonggi- do, Republic of Korea

2 Division of Biotechnology, The Catholic University of Korea, 43 Jibong-ro, Bucheon-si 14662, Gyeonggi-do, Republic of Korea

3 College of Pharmacy, Chung-Ang University, 84 Heukseok-ro, Dongjak-gu, Seoul 06974, Republic of Korea

4 College of Pharmacy, Hanyang University, 55, Hanyangdaehak-ro, Sangnok-gu, Ansan 15588, Republic of Korea

an increased maximum tolerated dose (Kratz 2008; Lee and Youn 2016).

Hyperthermia can be used as a promising tool in cancer therapy because cancer cells are vulnerable to heat and temperature increases (Kang et al. 2020; Kang and Kim 2020). According to many works in the literature, cancer cells experience irreversible damage when at > 48 °C for a few minutes and at 42–48 °C for > 1 h. Furthermore, incremental temperature increases around 41–42 °C, called moderate hyperthermia, can be applied to expand tumor blood vessels, thereby facilitating delivery of chemotherapeutic agents to tumor regions (Jaque et al. 2014). Among many near infrared (NIR) dyes having hyperthermal effects, only indocyanine green (ICG) is clinically available (Hill et al. 2015; Shimizu et al. 1995). Recently, many approaches based on nanotechnology have been used to solve the physicochemical problems such as poor stability and aggregation of ICG (Desmettre et al. 2000; Sheng et al. 2014; Mundra et al. 2015).

Most solid tumors develop extensive fibrotic physiological regions called the extracellular matrix (ECM) (Whatcott et al. 2011). This abnormal connective stroma is composed of various ECM components such as hyaluronic acid (HA), collagen, fibronectin, and laminin (Eble and Niland 2019). ECM plays a critical role in increasing interstitial fluid pressure (IFP) and in hindering the penetration of anticancer agents (Prabhakar et al. 2013). Therefore, destroying the ECM components can be a good approach to deliver chemotherapeutic drugs to tumors and to overcome chemoresistance. Among the ECM components, HA, a linear polysaccharide composed of glucuronic acid and N-acetylglucosamine, dramatically develops in cancers, whereas the level of hyaluronic acid is generally quite low in most normal tissue (Nagy et al. 2015). Since HA acts as a molecular strainer that hinders the penetration of drugs, treatment with hyaluronidase (HAase), which degrades HA, may increase the penetration of drugs through the stromal ECM and eventually into tumor cells (Toole 1973; Styles et al. 2019).

Previously, we developed a variety series of Nab™ technique-based albumin nanoparticle formulations (with hyperthermal activity or embedded with other functional proteins) for treating many cancers (Min et al. 2015; Byeon et al. 2016; Kim et al. 2017; Lee et al. 2017). Herein, albumin-bound nanoparticles were considered to be the best template formulation in an attempt to simultaneously achieve cytotoxic effects, hyperthermia and HA-degrading ability in a single nanostructure. Therefore, we designed and fabricated the Abraxane^{TM}-like albumin nanoparticles containing PTX, ICG and HAase (hereafter termed PTX/ICG/HAase-HSA-NPs). The physicochemical properties of PTX/ICG/HAase-HSA-NPs were investigated using relevant spectroscopic analyses. The cancer cell cytotoxicities of these NPs were evaluated using human pancreatic adenocarcinoma AsPC-1 cells and their 3D spheroids.

Materials and methods

Materials

Paclitaxel was obtained from JW Pharmaceutical Corporation (Dangjin, South Korea). ICG was purchased from Tokyo Chemical Industry Co., LTD, (TCI, Japan). Human serum albumin, hyaluronidase (HAase), and RPMI were purchased from Sigma-Aldrich (St. Louis, MO, USA). AsPC-1 cells were purchased from the Korean Cell Line Bank (Seoul, Korea). Fetal bovine serum (FBS) was purchased from Capricorn (Ebsdorfergrund, Hesse, Germany). Trypsin-EDTA and penicillin-streptomycin solution were purchased from Corning (Corning, NY, USA). The LIVE/DEAD® viability/cytotoxicity assay kit was purchased from Thermo Fisher Scientific (Rockford, IL, USA). LysoTracker® Green DND-26 was obtained from Life Technologies (Eugene, OR, USA). All other reagents were obtained from Sigma-Aldrich unless otherwise indicated.

Fabrication of PTX/ICG/HAase-HSA-NPs

PTX-HSA-NPs, PTX/ICG-HSA-NPs, and PTX/ICG/HAase-HSA-NPs were prepared using the previously described methods based on the nanoparticle albumin-bound (Nab™) technique with slight modifications (Kim et al. 2017; Phuong et al. 2018). Briefly, aliquots of 50 mg HSA, 50 mg HSA/1.5 mg ICG and 50 mg HSA/HAase (1, 2, 5 mg) were dissolved in 5 mL deionized water (DW). Aliquots (5 mg) of PTX were dissolved in 100 µl of a 9:1 solution of chloroform and ethanol. Solutions of each set of aqueous/organic phase were gently mixed and homogenized using a Wise Tis homogenizer HG-15D (DAIHAN Scientific Co, Seoul, South Korea) at 14,500 rpm for 3 min and then passed through a high-pressure homogenizer (EmulsiFlex-B15 device Avestin, Ottawa, Ontario, Canada) for nine cycles at 20,000 psi (Table 1). After removal of chloroform by a rotary evaporator at 40 °C for 15 min under reduced pressure, the resulting NPs were mildly centrifuged at 6,000 rpm. The supernatant was collected and purified with Ultra centrifugal filter units (MWCO: 100 kDa, Amicon® Ultra, Millipore) to remove the unbound PTX, ICG, and HAase. Supernatant was then freeze-dried and stored at − 20 °C until needed.

Characterization of PTX/ICG/HAase-HSA-NPs

The average sizes and the zeta potentials of the PTX-HSA-NPs, PTX/ICG-HSA-NPs and PTX/ICG/HAase-HSA-NPs

Table 1 Formulation (target loading) and characterization results of HSA-NPs

HSA-NPs	HSA (mg)	ICG (mg)	PTX (mg)	Hyaluronidase (mg)	Size (nm)	PDI	Zeta potential (mV)
PTX/HSA-NPs	50	1.5	5	–	151.3 ± 30.4	0.066 ± 0.012	− 27.9 ± 1.3
PTX/ICG/HSA-NPs					149.6 ± 21.7	0.234 ± 0.015	− 36.7 ± 2.9
PTX/ICG/HAase/HSA-NPs				1, 2, 5	109.5 ± 21.4	0.336 ± 0.026	− 30.4 ± 1.8

(HAase 1, 2 and 5 mg) were measured using dynamic light scattering (Zetasizer Nano ZS90, Malvern Instruments, Worcestershire, UK) with a 633 nm He-Ne laser beam and a fixed 90° scattering angle. The surface morphology of the NPs was observed by transmission electron microscopy (TEM) with a model JEM-3010 (JEOL, Tokyo, Japan) and field-emission scanning electron microscopy (FE-SEM) using a JSM7000F model (JEOL, Tokyo, Japan). The physical stability of the NPs was evaluated by considering the stability of the particle size. Briefly, the particle sizes of PTX/HSA-NPs and PTX/ICG/HAase-HSA-NPs were monitored at 1, 2, 3, 6, 9, 12, 18, 24, 30, 36, 42, and 48 h using the DLS method described above. UV–VIS–NIR spectral scans of the HSA-NPs samples were also recorded with a Synergy™ NEO microplate reader (Bio Tek, Winooski, VT, USA). Separately, circular dichroism (CD) spectra from PBS, free ICG, PTX-HSA-NPs, PTX/ICG-HSA-NPs and PTX/ICG/HAase-HSA-NPs were recorded at a concentration of 2 mg/mL in PBS buffer using a Dichroism Spectropolarimeter (J-1500, Jasco International Co., Ltd., USA). The far UV region was scanned between 190 nm and 250 nm.

Determination of loading efficiency and release of PTX and ICG

The loading efficiency of PTX and ICG in PTX/ICG/HAase-HSA-NPs was evaluated using the following protocol. Briefly, 1 mg of the lyophilized PTX/ICG/HAase-HSA-NP was dissolved in 0.1 mL DW. To remove HSA and hyaluronidase from the NPs, 0.9 ml acetonitrile (ACN) was added to the NP suspension, followed by sonication for 30 min and centrifugation at 14,500 rpm for 20 min. Subsequently, the supernatant was withdrawn for quantification. UV absorption spectrophotometry at 808 nm was used to measure ICG concentration, while fluorescence spectrophotometry was conducted at excitation and emission wavelengths of 420 and 526 nm. To determine the loading efficiency of PTX, the supernatant was subjected to reverse-phase high performance liquid chromatography (RP-HPLC) using a PLRP-S Zorbax 100 RP-18 column (150 mm × 4.6 mm, 8 µm/300 Å; Agilent Technologies, Palo Alto, CA, USA) at ambient temperature. A combined gradient plus isocratic elution method was carried out at a flow-rate of 1.0 mL /min using solvent A (DW) and solvent B (ACN); that is, 0–60% B for 7 min, 60% B for 10 min, and 100% A for 4 min. Eluates were monitored at 223 nm. Three replicates of each sample were prepared and analyzed (n = 03).

To investigate the PTX and ICG release profiles from the HSA-NPs, 20 mg of PTX/ICG/HAase-HSA-NPs was dissolved in 2 mL 10 mM PBS (pH 7.4) and dialyzed using a semipermeable 10 kDa MWCO membrane (Spectrum Labs, Rancho Dominguez, CA, USA) against 1 L of 10 mM PBS (pH 7.4) at 37 °C. Every 3 h over 48 h, 0.1 mL of the sample inside the dialysis bag was withdrawn and quantified by the methods mentioned above.

Monitoring of NIR-induced hyperthermia of PTX/ICG/HAase-HSA-NPs

For the photothermal imaging experiments, 1 mL aliquots of PBS, free IGC (20 µg/ mL) and PTX/ICG/HAase-HSA-NPs (approximately 20 µg/ mL equivalent ICG) were assessed in 1.5 mL eppendorf tubes and exposed to laser irradiation (808 nm, 1.5 W/cm^2) over 4 min. The laser spot size was ~ 1.0 cm^2. The temperature changes were recorded and observed using a FLIR E85 photothermal camera (FLIR Systems, Inc., Wilsonville, U.S.A.).

Cytotoxicity evaluation of PTX-HSA-NPs and PTX/ICG/HAase-HSA-NPs

The toxicity of PTX/HSA-NPs, PTX/HAase/HSA-NPs, PTX/ICG/HSA-NPs and PTX/ICG/HAase-HSA-NPs with various loading amounts of HAase (1, 2 and 5 mg) with or without laser irradiation were evaluated using two separate assays of the MTT and LIVE/DEAD® assays. First, an MTT colorimetric assay was conducted using a slight modification of previous methods (Kim et al. 2017; Lee et al. 2017; Park et al. 2019; Seo et al. 2019). Briefly, AsPC-1 cells were seeded in 96-well plates at a density of 1×10^4 cells/well in RPMI media containing 10% (v/v) fetal bovine serum and 1% penicillin/streptomysin in a 5% CO_2, 95% RH incubator at 37 °C. Following a 24 h incubation, the cells were treated with various concentrations of PTX/HSA-NPs, PTX/HAase/HSA-NPs, PTX/ICG/HSA-NPs, and PTX/ICG/HAase-HSA-NPs. Afterward, the cells were incubated for 24 h and treated with or without laser irradiation (808 nm, 1.5 W/cm^2 for 5 min). The cells were then incubated for an

additional 24 h. In vitro cytotoxicity was determined using a 3-(4,5-dimethylthiazol-2-yl)-2,5-diphenyltetrazolium bromide (MTT)-based assay.

A LIVE/DEAD® viability/cytotoxicity kit was applied to visualize the live and dead cells more clearly. AsPC-1 cells were seeded to wells on an 8-well chamber (Ibidi, Martinsried, Germany) at 1.5×10^4 cells/well. Twenty-four hours after seeding, the cells were treated with PTX/HSA-NPs, PTX/ICG/HSA-NPs and PTX/ICG/HAase-HSA-NPs with various hyaluronidase concentrations (at the equivalent of ~200 ng/mL of PTX). After 72 h of incubation, the cell media were replenished with DPBS before irradiation with or without a laser. Cells were incubated for an additional 24 h and then collected to label live/dead dyes (live cells were stained green with Calcein-AM, while dead ones were stained red with ethidium homodimer-1). Finally, the stained cells were observed by confocal laser scanning microscopy (CLSM; LSM510, Carl Zeiss Meditec AG, Jena, Germany) at excitation and emission wavelengths of 494 and 517 nm, respectively, for Calcein-AM and 528 and 617 nm, respectively, for ethidium homodimer-1.

Evaluation of PTX/ICG/HAase-HSA-NPs uptake into AsPC-1 cells and spheroids

To examine cellular uptake, AsPC-1 cells were cultured as 2D monolayers and 3D spheroids. To create 2D monolayers, 100 µL aliquots of AsPC-1 cells (1.5×10^4 cells per well) were added to wells of an 8-well chamber (Ibidi, Martinsried, Germany). Sampled 2D monolayers were also rinsed three times with DPBS after drug treatment for one day and were incubated for 60 min with 50 nM LysoTracker Green to visualize lysosomes. Then, cells were rinsed three more times with DPBS and fixed with 4% paraformaldehyde in PBS for 20 min. Finally, the cells were washed and treated with a 4′,6-diamidino-2-phenylindole solution (DAPI) to observe nuclei. Cellular uptake of PTX/ICG/HAase-HSA-NPs into AsPC-1 cells was visualized by confocal laser scanning microscopy (CLSM; LSM510, Carl Zeiss Meditec AG, Jena, Germany). For spheroids, AsPC-1 cells (5,000 cells per well) were seeded in cell plates designed to induce the formation of 3D multicellular spheroids (Shimadzu, Kyoto, Japan). The cell spheroids were established over 3 days and were then treated with PTX/ICG/HAase-HSA-NPs containing 10 µg/mL of ICG followed by a 24-h incubation. After incubation, the spheroids were washed three times with ice-cold DPBS and transferred to an 8-well chamber (Ibidi, Martinsried, Germany) to be observed by confocal microscopy using the z-stack image collection mode (10 µm step size, ~100 µm in depth).

Data analysis

Data are presented as the mean ± standard deviation (SD). Significant differences were determined using Student's t-tests. P-values < 0.05 were considered statistically significant.

Results

Preparation and characterization of the PTX/ICG/HAase/HSA-NPs

PTX/ICG/HAase/HSA-NPs were prepared using a high-pressure homogenizer based on the Nab™ technique (Fig. 1). Abraxane®-like albumin nanoparticles provide a good pharmaceutical advantage in terms of loading various type of drugs, e.g., chemicals and other therapeutic or functional proteins (Byeon et al. 2016; Lee et al. 2017; Min et al. 2015). In this nanostructure, three components of PTX, ICG and HAase were used to suppress pancreatic cancers, induce hyperthermia and destroy hyaluronic acid in ECM. The size of prepared PTX/HSA-NPs, PTX/ICG/HSA-NPs and PTX/ICG/HAase/HSA-NPs were shown to be 151.3 ± 30.4, 149.6 ± 21.7 nm, and 109.5 ± 21.4 nm, respectively. The zeta potentials of the PTX/HSA-NPs, PTX/ICG/HSA-NPs, and PTX/ICG/HAase/HSA-NPs were found to be -27.9 ± 1.3 mV, -36.7 ± 2.9 mV, and − 30.4 ± 1.8 mV, respectively (Fig. 2a). The polydispersity indices (PDI) of the PTX/HSA-NPs, PTX/ICG/HSA-NPs, and PTX/ICG/HAase/HSA-NPs were 0.066 ± 0.012, 0.234 ± 0.015, and 0.336 ± 0.026,

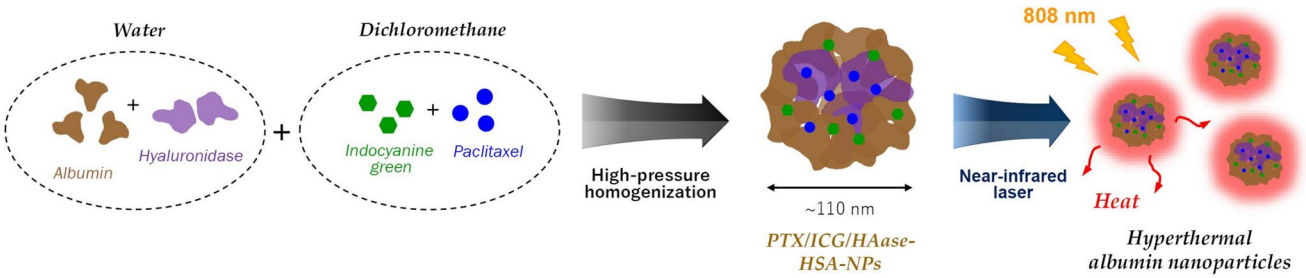

Fig. 1 Schematic illustration of the design and preparation of PTX/ICG/HAase-loaded albumin nanoparticles

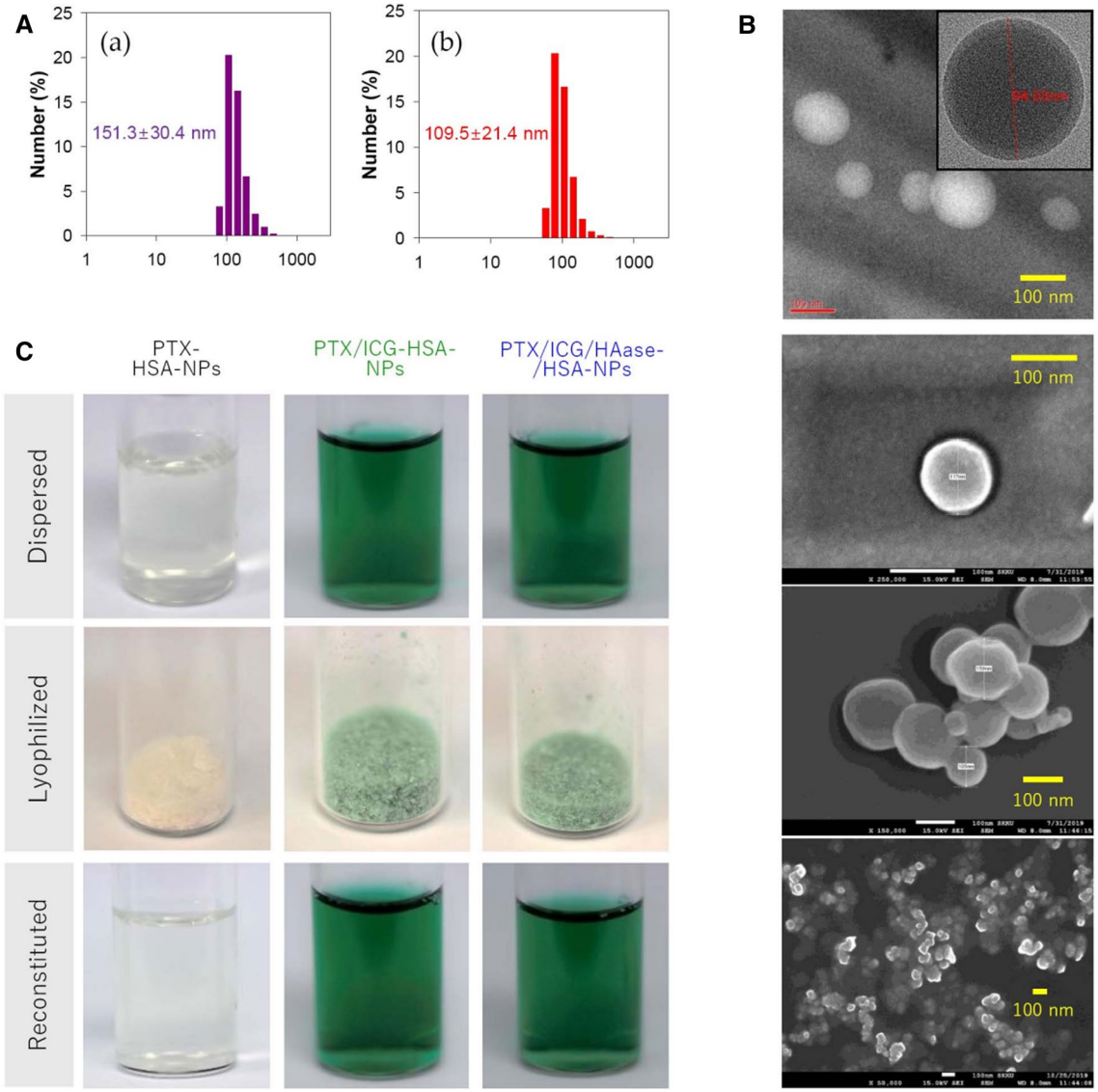

Fig. 2 **a** Histograms of particle sizes of PTX-HSA-NPs and PTX/ICG/HAase-HSA-NPs, **b** TEM (top) and FE-SEM images of PTX/ICG/HAase-HSA-NPs. **c** Photographs of the solution (top), lyophilized powder (middle), and reconstituted suspension (bottom) of the PTX-HSA-NPs, PTX/ICG-HSA-NPs and PTX/ICG/HAase-HSA-NPs

respectively. The feed amount of HAase slightly increased the zeta potentials (Fig. 3a). The TEM and FE-SEM images showed that these nanoparticles were spherical and highly homogenous in size (Fig. 2b).

Stability of the PTX/ICG/HAase/HSA-NPs

The stability of the PTX/HSA-NPs and PTX/ICG/HAase/HSA-NPs were evaluated over 48 h in terms of ability to maintain particle size. As shown in Fig. 3b, the particle sizes of the PTX/HSA-NPs and PTX/ICG/HAase/HSA-NPs were relatively well maintained over this time period. All HSA-NP fabricated samples (PTX/HSA-NPs, PTX/ICG/HSA-NPs, and PTX/ICG/HAase/HSA-NPs) dispersed well, and their colloidal dispersions after reconstitution appeared to be clear, similar to those before lyophilization, indicating good nanoparticle stability (Fig. 3c).

Absorbance profiles of PTX/ICG/HAase/HSA-NPs in UV–VIS–NIR and circular dichroism spectra

The UV–VIS–NIR absorbance spectra of free ICG, PTX-HSA-NPs, PTX/ICG/HSA-NPs, and PTX/ICG/HAase/HSA-NPs with different hyaluronidase amounts (1, 2 and 5 mg) were observed in the wavelength range from 300 to 900 nm. As shown in Fig. 3c, the albumin nanoparticle groups including ICG (free ICG, PTX/ICG/HSA-NPs, and PTX/ICG/HAase/HSA-NPs) had significant spectral peaks

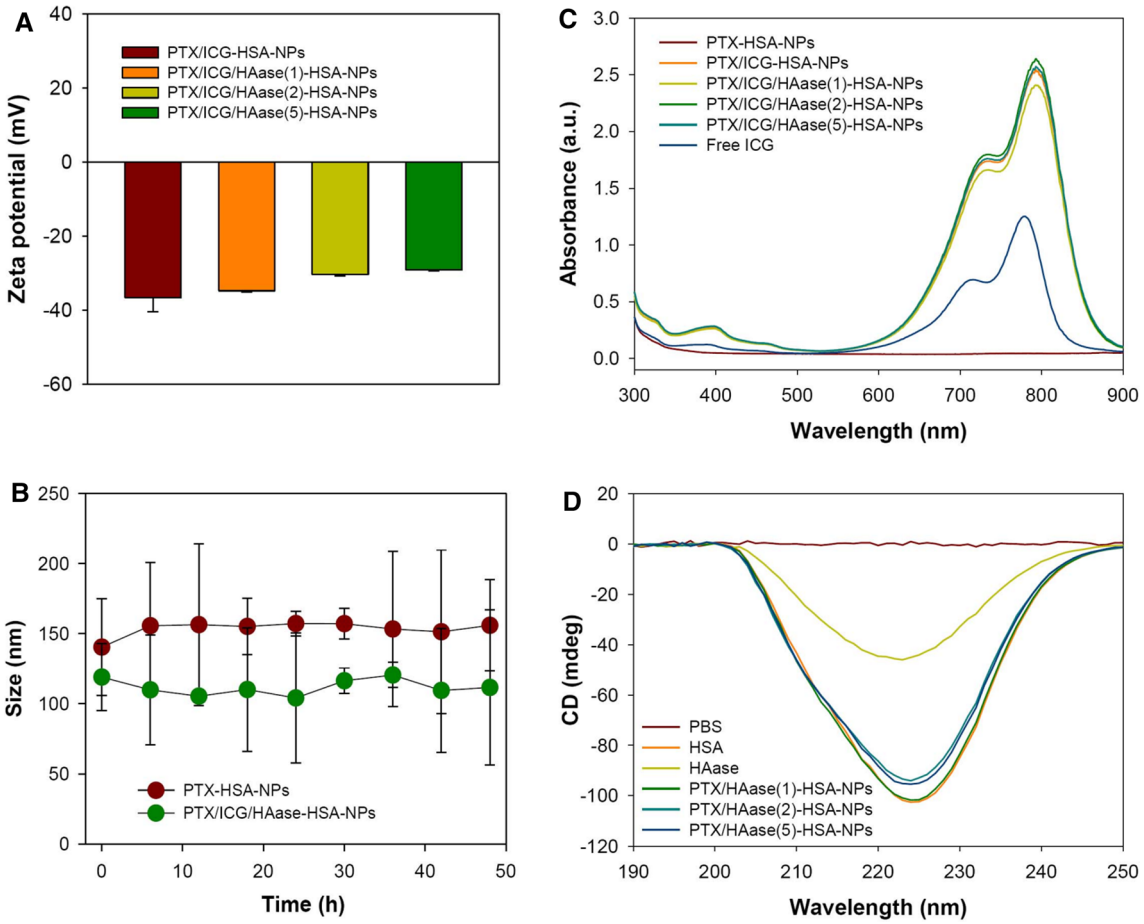

Fig. 3 **a** Zeta potentials of PTX-HSA-NPs and PTX/ICG/HAase-HSA-NPs (1, 2 and 5 mg HAase). **b** Physical stability of PTX-HSA-NPs and PTX/ICG/HAase-HSA-NPs based on size changes. **c** UV–VIS–NIR absorption spectra of free ICG, PTX/ICG-/HSA-NPs and PTX/ICG/HAase-HSA-NPs (1, 2 and 5 mg HAase). **d** Circular dichroism spectra of PBS, HSA, HAase, and PTX/ICG/HAase-HSA-NPs (1, 2 and 5 mg HAase) (top)

around 800 nm, which corresponded to the typical absorbance spectrum of ICG, whereas unmodified PTX-HSA-NPs showed no significant spectral pattern. The CD spectra for PTX/ICG/HAase/HSA-NPs changed little regardless of hyaluronidase addition and were similar to those of neat HSA and hyaluronidase, showing the highest negative peak around 225 nm (Fig. 3d).

PTX and ICG release from PTX/ICG/HAase/HSA-NPs

PTX and ICG are known to bind to albumin by strong non-covalent interactions between the aromatic and heteroaromatic rings of ICG and the hydrophobic pockets of albumin. PTX and ICG appeared to gradually release from HSA-NPs over time, presumably due to looser bonds. The in vitro release profiles of PTX and ICG from PTX/ICG/HAase/HSA-NPs were observed over 48 h. The PTX release was much faster than that of ICG, indicating almost 90% PTX release within 15 h (Fig. 4a). In contrast, ICG was gradually released from PTX/ICG/HAase/HSA-NPs, while 80% of the incorporated ICG was slowly released over 48 h (Fig. 4b). However, the 808 nm laser irradiation promoted significantly faster release of both PTX and ICG. Approximately 75% of PTX and 60% of ICG were released in 1 h. This appeared to be due to loosening of the physical bonds between PTX/ICG and the associated albumin molecules or partial degradation of HSA-NPs due to the increased temperature in HSA-NPs upon 808 nm laser irradiation.

Hyperthermal effect of PTX/ICG/HAase/HSA-NPs

PTX/ICG/HAase/HSA-NPs displayed obvious temperature increases in response to laser irradiation, unlike the PTX/HSA-NPs without ICG. The heat generation and temperature increase of ICG was proportional to the amount of ICG and irradiation time of the 808 laser. The temperatures of the PTX/ICG/HAase/HSA-NPs (1, 2 and 5 mg of HAase) reached peak temperatures of 59.3, 58.5 and 55.8 °C at

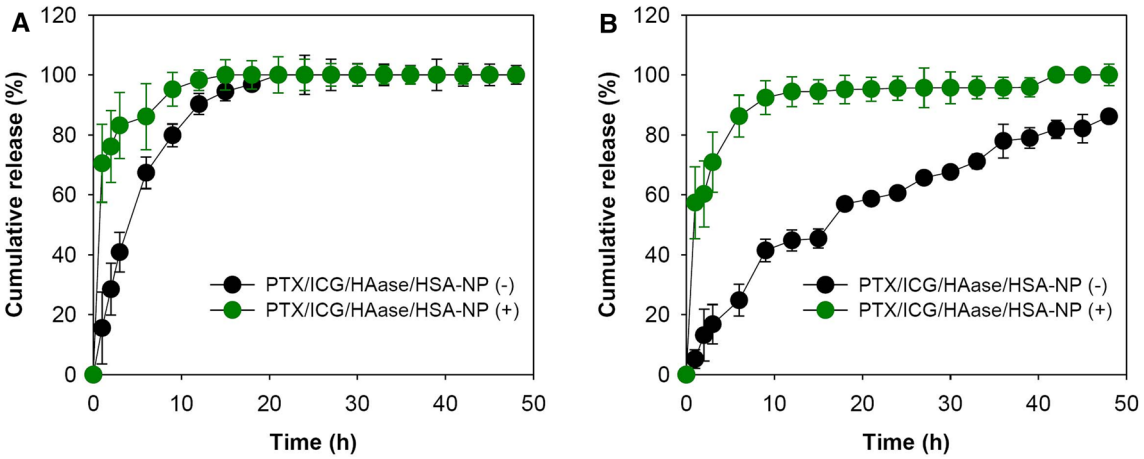

Fig. 4 In vitro release profiles of **a** PTX and **b** ICG from PTX/ICG/HAase-HSA-NPs (+ 808 nm or – 808 nm)

4 min after irradiation, respectively, compared with 64.5 °C of ICG alone (20 μg/ml) (Fig. 5a. However, the temperature of HSA/PTX-NPs and PBS remained steady at around 30 °C upon laser irradiation. These clear temperature changes were verified visually using a photothermal camera, which shows the strong color intensity of ICG-containing HSA-NP groups (Fig. 5b).

Cytotoxicity of PTX/ICG/HAase/HSA-NPs towards AsPC-1 cells

Two separate assays were conducted to achieve comprehensive cytotoxic evaluations of PTX/ICG/HAase/HSA-NPs. First, the MTT results illustrated that the 808 nm laser irradiation resulted in significantly higher cytotoxicity of PTX/ICG/HAase/HSA-NPs to AsPC-1 cells (Fig. 6a). The PTX/ICG/HAase/HSA-NPs killed approximately 50% of AsPC-1 cells at 100 ng/ mL without the 808 nm laser. However, when irradiated, 60–80% of cells were killed at concentrations of 0.001–10 ng/ mL. When using irradiation under temperature-controlled conditions (41–42 °C), fewer cells seemed to be killed at 20 min laser exposure. Consequently, the temperature difference resulted in cell death (29.9% vs. 19.3%; $P < 0.05$) (Fig. 6b).

The same pattern in cytotoxicity to AsPC-1 cells was observed in the live/dead assay. The control PBS group showed no cell death as visualized by green fluorescence. Half of the cells were killed by PTX when treated with PTX/HSA-NPs without an 808 nm laser (Fig. 7 left). Similarly, treatment with PTX/ICG/HSA-NPs and PTX/ICG/HAase/HSA-NPs in the absence of laser irradiation resulted in partial cell death, as indicated by a red or green fluorescence

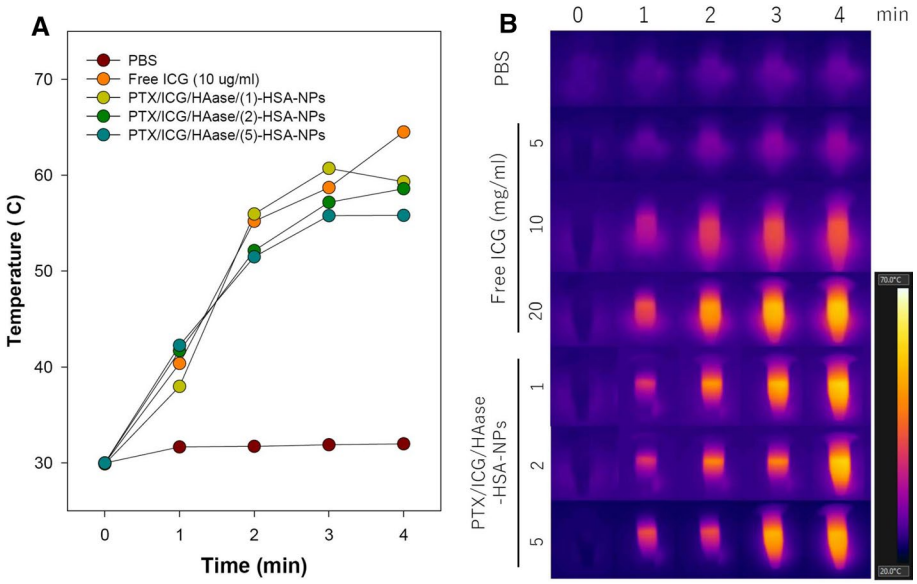

Fig. 5 **a** Surface temperature profiles of PBS, free ICG (10 μg/ mL), PTX/ICG/HAase-HSA-NPs (1, 2 and 5 mg HAase fed; ICG 10 μg/ mL) over 4 min upon NIR laser irradiation (808 nm, 1.5 W/cm^2). **b** Thermographic images of free ICG with different concentrations (5, 10 and 20 μg/ mL) and PTX/ICG/HAase-HSA-NPs (1, 2 and 5 mg HAase fed; ICG 10 μg/ mL) after NIR laser irradiation (808 nm, 1.5 W/cm^2)

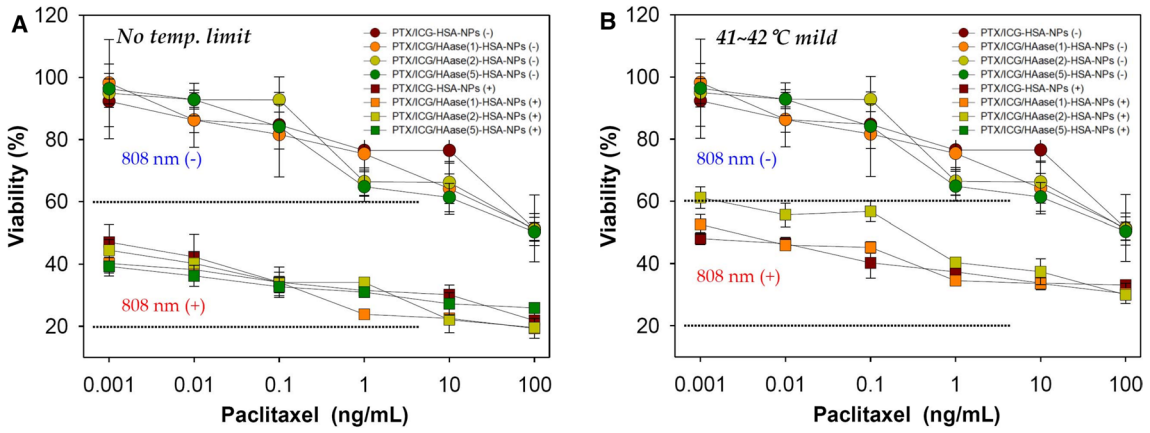

Fig. 6 MTT assay-based cytotoxicity of PTX/ICG-HSA-NPs and PTX/ICG/HAase-HSA-NPs (1, 2 and 5 mg HAase) in AsPC-1 cells. **a** Cytotoxicity with or without irradiation of an 808 nm NIR laser (808 nm 1.5 W/cm^2, 10 min): no temperature limit (50–51 °C). **b** Cytotoxicity with or without irradiation of an 808 nm NIR laser (808 nm 1.5 W/cm^2, 10 min): controlled surface temperatures up to 41–42 °C

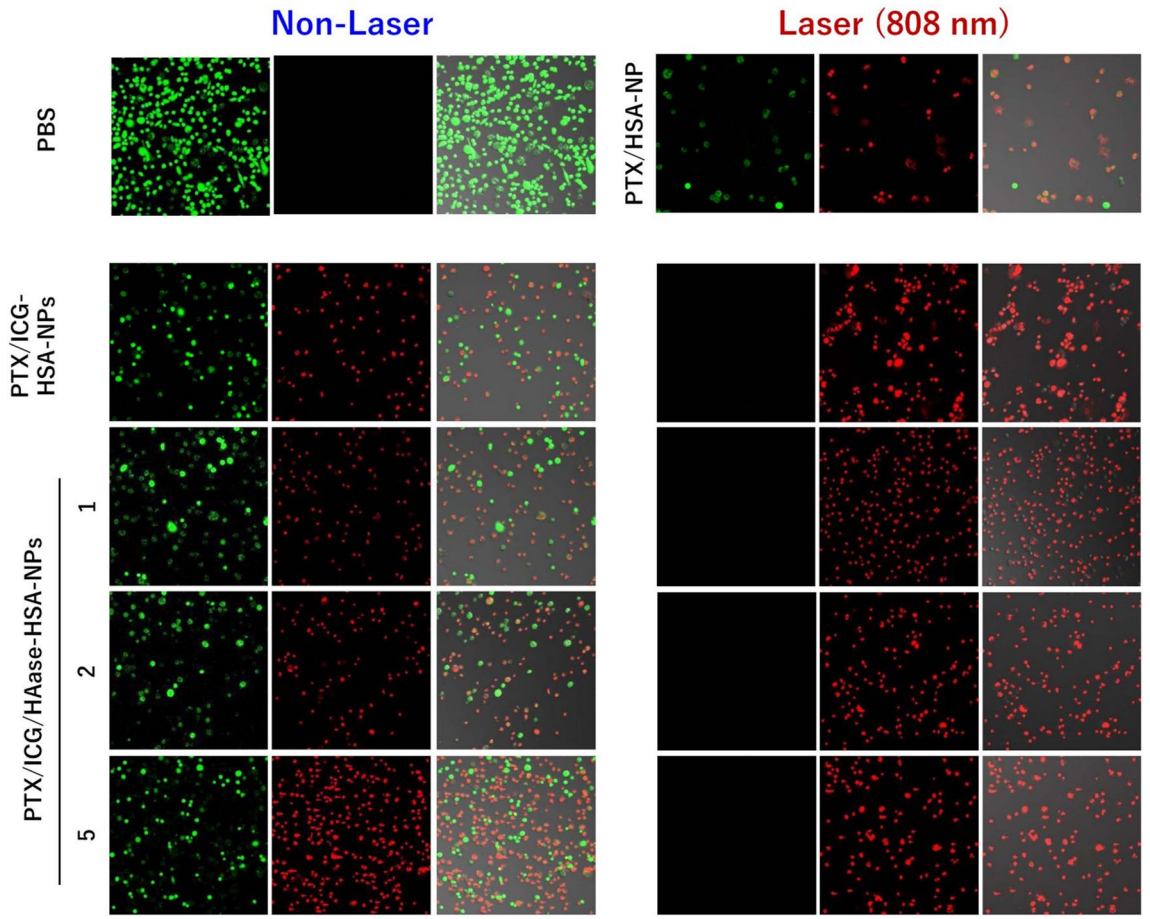

Fig. 7 LIVE/DEAD® assay for AsPC-1 cells incubated with PBS, PTX-HSA-NPs, PTX/ICG-HSA-NPs and PTX/ICG/HAase-HSA-NPs (1, 2 and 5 mg HAase) with or without laser irradiation (808 nm 1.5 W/cm^2, 15 min)

signal. ICG alone seemed to have no significant toxicity for the cells without NIR light, and HAase did not affect cellular toxicity. In contrast, almost all cells seemed to be killed after treatment with PTX/ICG/HSA-NPs and PTX/ICG/HAase/HSA-NPs followed by 808-nm laser irradiation, as visualized by red staining (Fig. 7 right).

CLSM visualization of AsPC-1 cellular uptake of PTX/ICG/HAase/HSA-NPs

The uptake of PTX/ICG/HAase/HSA-NPs into AsPC-1 2D monolayers and 3D spheroids was observed by CLSM. As shown in Fig. 8, the ICG fluorescence induced by PTX/ICG/HAase/HSA-NPs appeared to be superimposed with that of the Lysotracker at 1–12 h in AsPC-1 cells. This indicated that PTX/ICG/HAase/HSA-NPs were taken up by the cells at 1 h and localized around lysosomes in the cells. Uptake of fabricated nanoparticles were examined at different time intervals (30 min, 1, 2, 3, 6, 12 h). To better understand the uptake of PTX/ICG/HAase/HSA-NPs in pancreatic tumors, a spheroid model was utilized in this study. Actually, tumor microenvironments present significant barriers to macromolecules and nanoparticle penetration. Cancer cells cultured as 2D monolayers were more sensitive to toxic materials than those grown in vivo. Therefore, 3D spheroids can be a better option for in vivo tumor tissues (Choi et al. 2015). AsPC-1 cell spheroids were incubated with PTX/ICG/HAase/HSA-NPs for 24 h. As shown in Fig. 9, the diameter of AsPC-1 spheroids was about 450 μm, and the confocal spectroscopic images of AsPC-1 cell spheroids obtained from slices with a 10-μm step size showed clear green fluorescence, indicating that PTX/ICG/HAase/HSA-NPs were clearly internalized into the spheroids. These results might imply that PTX/ICG/HAase/HSA-NPs would be able to permeate into three-dimensional tumor tissues in vivo.

Discussion

The clinical use of engineered nanoparticles is a valid method for targeted drug delivery in cancer therapy (Arpagaus 2019; Lee et al. 2019; Tran et al. 2019; Asadujjaman et al. 2020; Dai Phung et al. 2020; Jo et al. 2020; Kim et al. 2020; Le and Youn 2020). Among many nanoparticle platforms, such as, organic, metal or hybrid nanoparticles, protein-based nanoparticles, have many pharmaceutical advantages over the others (Lohcharoenkal et al. 2014). Especially,

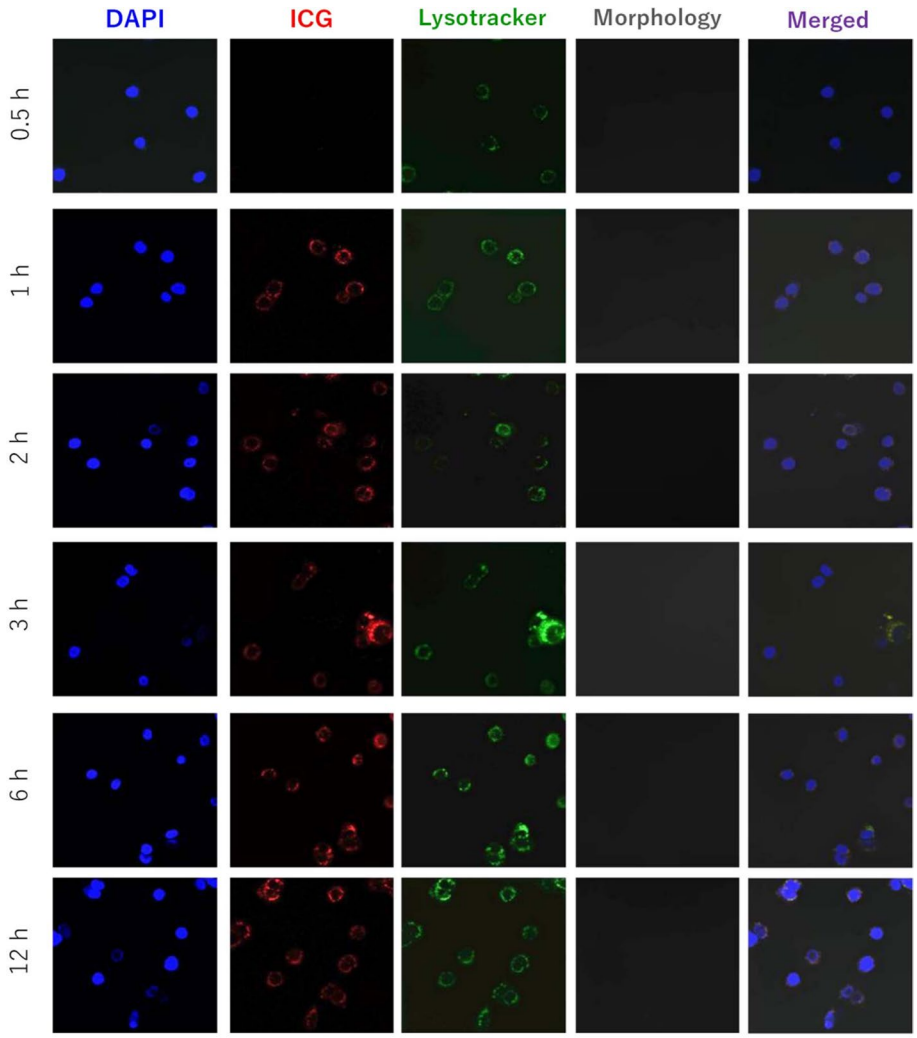

Fig. 8 Uptake of PTX/ICG/HAase-HSA-NPs into AsPC-1 cells. Cells were treated with PTX/ICG/HAase-HSA-NPs (HAase 1 mg fed; ~200 ng/mL PTX)

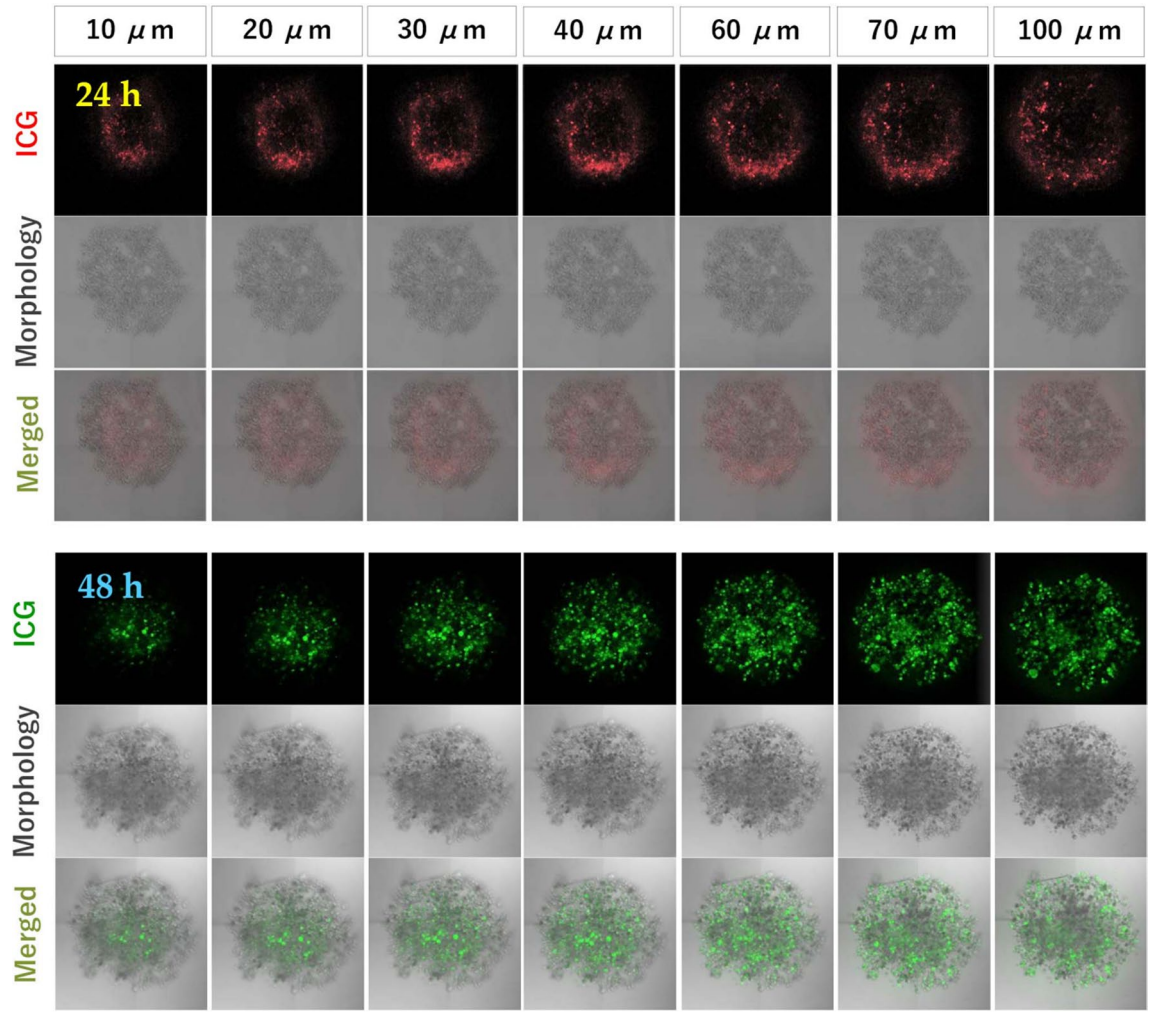

Fig. 9 Permeability of PTX/ICG/HAase-HSA-NPs into AsPC-1 3D spheroids. Spheroids were treated with PTX/ICG/HAase-HSA-NPs (~200 ng/mL PTX). At 24 h (top) and 48 h (bottom) after the treatment, the z-stack images of 10 slices that were 10 μm in thickness were obtained

albumin-based nanoparticles can be considered a high priority choice for clinical use, whereas many other nanomaterials have considerable toxicity, poor biocompatibility and safety (Kratz 2014). On this basis, we chose human serum albumin as a main building material to design and prepare our nanoparticle structure. Among the many methods to make albumin nanoparticles (Elzoghby et al. 2012), Abraxane®-like albumin nanoparticles were considered to be the best option because they are physically crosslinked via hydrophobic interactions and thus facilely dissociate to smaller particle species or albumin molecules, which is favorable compared to extravasation/accumulation of anticancer drugs into tumor tissues (Youn and Bae 2018). Consequently, we thought that the fabricated albumin nanoparticles are able to pass through endothelia cells and target solid tumors.

Heat generation is a significant parameter for photothermal efficiency. In this study, ICG was chosen as a fluorescent and photothermal agent because it has many advantages. It has low toxicity, is clinically available and highly absorbs light from 650 to 950 nm, which is a relatively transparent window for biological tissues (Yuan et al. 2004; Avci et al. 2013). This is known as the therapeutic window that allows high photothermal efficiency without harming normal tissues (Sordillo et al. 2014). Deep red NIR lasers from 650 to 950 nm penetrate tissues 2–3 mm in depth compared with 0.5–1.0 and 1.0–2.0 mm for 545 to 600 nm and 600 to 650 nm, respectively (Avci et al. 2013). As shown in Fig. 6a and b, our PTX/ICG/HAase/HSA-NPs strongly absorbed 808 nm-light, and this absorption converts photoenergy into thermal energy, damaging surrounding cells via heat. Especially, the incorporation of HAase or PTX seemed not to negatively affect the photothermal efficiency.

This burst release can often be regarded as a negative response that is detrimental to maintaining long-term

controlled release. In contrast, it can also be applied to the planned and concentrated release of PTX in terms of controllable drug initiation by laser irradiation/heat induction (Huang 2001), which was considered more beneficial to our anticancer targeting system. Moreover, the incorporation of ICG and HAase did not affect their cell cytotoxicity irrespective of the amount of HAase. In this study, the hyperthermal degree was determined to be severe (> 50 °C) and mild (41–42 °C), and these conditions have different degrees of killed cancer cells depending upon laser irradiation time. Mild hyperthermia can be used for dilating endothelial vessel around tumors to increase the delivery of anticancer nanoparticles (Kang et al. 2020). Likewise, temperature-controlled hyperthermia can be utilized for different anticancer therapy purposes. To this end, our PTX/ICG/HAase/HSA-NPs were considered to be adequate for mild hyperthermal and chemotherapeutic properties on the basis of continuous drug release of PTX and ICG.

In conclusion, we developed a prototype of albumin nanoparticles that has potential therapeutic uses for chemotherapeutic efficacy, hyperthermal effect, and ECM-destroying activity. To this end, our Nab™ technology-based albumin nanoparticles contained paclitaxel, indocyanine green and hyaluronidase, respectively. PTX/ICG/HAase/HSA-NPs were ~ 110 nm in size, showed good colloidal stability, and provided a remarkable hyperthermal response to 808 nm NIR light that generated a sufficient heat and temperature increase (> 50 °C). Based on the cytotoxic effect observed in AsPC-1 cells and spheroids, our results suggested that PTX/ICG/HAase/HSA-NPs would be used as tumor ablating agents in combined antitumor therapeutic functions. Further, we expect that the anticancer effect of PTX/ICG/HAase-HSA-NPs will be more obvious when applied to an ECM-based xenograft tumor model in our future studies.

Acknowledgements This work was supported by the National Research Foundation of Korea(NRF) grant funded by the Korea government (MSIT) (No. NRF-2019R1A5A2027340), and a grant (16173MFDS542) from the Ministry of Food and Drug Safety in 2020.

Compliance with ethical standards

Conflict of interest Authors declare no conflict of interest.

References

Arpagaus C (2019) PLA/PLGA nanoparticles prepared by nano spray drying. J Pharm Invest 49:405–426. https://doi.org/10.1007/s40005-019-00460-0

Asadujjaman M, Cho KH, Jang DJ, Kim JE, Jee JP (2020) Nanotechnology in the arena of cancer immunotherapy. Arch Pharm Res 43:58–79. https://doi.org/10.1007/s12272-020-01207-4

Avci P, Gupta A, Sadasivam M, Vecchio D, Pam Z, Pam N, Hamblin MR (2013) Low-level laser (light) therapy (LLLT) in skin: stimulating, healing, restoring. Semin Cutan Med Surg 32:41–52

Bae S, Ma K, Kim TH, Lee ES, Oh KT, Park E-S, Lee KC, Youn YS (2012) Doxorubicin-loaded human serum albumin nanoparticles surface-modified with TNF-related apoptosis-inducing ligand and transferrin for targeting multiple tumor types. Biomaterials 33:1536–1546. https://doi.org/10.1016/j.biomaterials.2011.10.050

Byeon HJ, Lee S, Min SY, Lee ES, Shin BS, Choi H-G, Youn YS (2016) Doxorubicin-loaded nanoparticles consisted of cationic- and mannose-modified-albumins for dual-targeting in brain tumors. J Control Release 225:301–313. https://doi.org/10.1016/j.jconrel.2016.01.046

Choi SH, Byeon HJ, Choi JS, Thao L, Kim I, Lee ES, Shin BS, Lee KC, Youn YS (2015) Inhalable self-assembled albumin nanoparticles for treating drug-resistant lung cancer. J Control Release 197:199–207. https://doi.org/10.1016/j.jconrel.2014.11.008

Dai Phung C, Tran TH, Kim JO (2020) Engineered nanoparticles to enhance natural killer cell activity towards onco-immunotherapy: a review. Arch Pharm Res 43:32–45. https://doi.org/10.1007/s12272-020-01218-1

Desmettre T, Devoisselle J, Mordon S (2000) Fluorescence properties and metabolic features of indocyanine green (ICG) as related to angiography. Surv Ophthalmol 45:15–27. https://doi.org/10.1016/S0039-6257(00)00123-5

Eble JA, Niland S (2019) The extracellular matrix in tumor progression and metastasis. Clin Exp Metastasis 36:171–198. https://doi.org/10.1007/s10585-019-09966-1

Elzoghby AO, Samy WM, Elgindy NA (2012) Albumin-based nanoparticles as potential controlled release drug delivery systems. J Control Release 157:168–182. https://doi.org/10.1016/j.jconrel.2011.07.031

Hill TK, Abdulahad A, Kelkar SS, Marini FC, Long TE, Provenzale JM, Mohs AM (2015) Indocyanine green-loaded nanoparticles for image-guided tumor surgery. Bioconjug Chem 26:294–303. https://doi.org/10.1021/bc5005679

Huang X, Brazel C (2001) On the importance and mechanisms of burst release in matrix-controlled drug delivery systems. J Control Release 73:121–136. https://doi.org/10.1016/S0168-3659(01)00248-6

Jaque D, Maestro LM, Del Rosal B, Haro-Gonzalez P, Benayas A, Plaza J, Rodriguez EM, Sole JG (2014) Nanoparticles for photothermal therapies. Nanoscale 6:9494–9530. https://doi.org/10.1039/C4NR00708E

Jo MJ, Jin IS, Park C-W, Hwang BY, Chung YB, Kim J-S, Shin DH (2020) Revolutionizing technologies of nanomicelles for combinatorial anticancer drug delivery. Arch Pharm Res 43:100–109. https://doi.org/10.1007/s12272-020-01215-4

Kang C, Kim D (2020) Nanoconfinement-mediated cancer theranostics. Arch Pharm Res 43:110–117. https://doi.org/10.1007/s12272-020-01217-2

Kang JK, Kim JC, Shin Y, Han SM, Won WR, Her J, Park JY, Oh KT (2020) Principles and applications of nanomaterial-based hyperthermia in cancer therapy. Arch Pharm Res 43:46–57. https://doi.org/10.1007/s12272-020-01206-5

Kim B, Seo B, Park S, Lee C, Kim JO, Oh KT, Lee ES, Choi H-G, Youn YS (2017) Albumin nanoparticles with synergistic antitumor efficacy against metastatic lung cancers. Colloids Surf B Biointerfaces 158:157–166. https://doi.org/10.1016/j.colsurfb.2017.06.039

Kim J, Jo Y-U, Na K (2020) Photodynamic therapy with smart nanomedicine. Arch Pharm Res 43:22–31. https://doi.org/10.1007/s12272-020-01214-5

Kratz F (2008) Albumin as a drug carrier: design of prodrugs, drug conjugates and nanoparticles. J Control Release 132:171–183. https://doi.org/10.1016/j.jconrel.2008.05.010

Kratz F (2014) A clinical update of using albumin as a drug vehicle—a commentary. J Control Release 190:331–336. https://doi.org/10.1016/j.jconrel.2014.03.013

Lamichhane S, Lee S (2020) Albumin nanoscience: homing nanotechnology enabling targeted drug delivery and therapy. Arch Pharm Res 43:118–133. https://doi.org/10.1007/s12272-020-01204-7

Le XT, Youn YS (2020) Emerging NIR light-responsive delivery systems based on lanthanide-doped upconverting nanoparticles. Arch Pharm Res 43:134–152. https://doi.org/10.1007/s12272-020-01208-3

Lee ES, Youn YS (2016) Albumin-based potential drugs: focus on half-life extension and nanoparticle preparation. J Pharm Investig 46:305–315. https://doi.org/10.1007/s40005-016-0250-3

Lee C, Kim B, Lee S, Kim TH, Kim JO, Lee ES, Oh KT, Choi H-G, Yoo SD, Youn YS (2017) Doxorubicin and paclitaxel co-bound lactosylated albumin nanoparticles having targetability to hepatocellular carcinoma. Colloids Surf B 152:183–191. https://doi.org/10.1016/j.colsurfb.2017.01.017

Lee GH, Shin DH, Suh H-W, Lee J-Y, Lim SS, Kim J-S (2019) Liposomal formulation and pharmacokinetic study of CPD409, a novel sodium channel blocker. J Pharm Invest 49:565–573. https://doi.org/10.1007/s40005-019-00445-z

Lohcharoenkal W, Wang L, Chen YC, Rojanasakul Y (2014) Protein nanoparticles as drug delivery carriers for cancer therapy. BioMed Res Int 2014:1–12. https://doi.org/10.1155/2014/180549

Min SY, Byeon HJ, Lee C, Seo J, Lee ES, Shin BS, Choi H-G, Lee KC, Youn YS (2015) Facile one-pot formulation of TRAIL-embedded paclitaxel-bound albumin nanoparticles for the treatment of pancreatic cancer. Int J Pharm 494:506–515. https://doi.org/10.1016/j.ijpharm.2015.08.055

Mundra V, Peng Y, Rana S, Natarajan A, Mahato RI (2015) Micellar formulation of indocyanine green for phototherapy of melanoma. J Control Release 220:130–140. https://doi.org/10.1016/j.jconrel.2015.10.029

Nagy N, Kuipers HF, Frymoyer AR, Ishak HD, Bollyky JB, Wight TN, Bollyky PL (2015) 4-methylumbelliferone treatment and hyaluronan inhibition as a therapeutic strategy in inflammation, autoimmunity, and cancer. Front Immunol 6:123. https://doi.org/10.3389/fimmu.2015.00123

Park S, Kim H, Lim SC, Lim K, Lee ES, Oh KT, Choi H-G, Youn YS (2019) Gold nanocluster-loaded hybrid albumin nanoparticles with fluorescence-based optical visualization and photothermal conversion for tumor detection/ablation. J Control Release 304:7–18. https://doi.org/10.1016/j.jconrel.2019.04.036

Phuong PTT, Lee S, Lee C, Seo B, Park S, Oh KT, Lee ES, Choi H-G, Shin BS, Youn YS (2018) Beta-carotene-bound albumin nanoparticles modified with chlorin e6 for breast tumor ablation based on photodynamic therapy. Colloids Surf B 171:123–133. https://doi.org/10.1016/j.colsurfb.2018.07.016

Prabhakar U, Maeda H, Jain RK, Sevick-Muraca EM, Zamboni W, Farokhzad OC, Barry ST, Gabizon A, Grodzinski P, Blakey DC (2013) Challenges and key considerations of the enhanced permeability and retention effect for nanomedicine drug delivery in oncology. Cancer Res 73:2412–2417. https://doi.org/10.1158/0008-5472.CAN-12-4561

Seo B, Lim K, Kim SS, Oh KT, Lee ES, Choi H-G, Shin BS, Youn YS (2019) Small gold nanorods-loaded hybrid albumin nanoparticles with high photothermal efficacy for tumor ablation. Colloids Surf B 179:340–351. https://doi.org/10.1016/j.colsurfb.2019.03.068

Sheng Z, Hu D, Zheng M, Zhao P, Liu H, Gao D, Gong P, Gao G, Zhang P, Ma Y (2014) Smart human serum albumin-indocyanine green nanoparticles generated by programmed assembly for dual-modal imaging-guided cancer synergistic phototherapy. ACS Nano 8:12310–12322. https://doi.org/10.1021/nn5062386

Shimizu S, Kamiike W, Hatanaka N, Yoshida Y, Tagawa K, Miyata M, Matsuda H (1995) New method for measuring ICG Rmax with a clearance meter. World J Surg 19:113–118

Sordillo LA, Pu Y, Pratavieira S, Budansky Y, Alfano RR (2014) Deep optical imaging of tissue using the second and third near-infrared spectral windows. J Biomed Opt 19:056004. https://doi.org/10.1117/1.JBO.19.5.056004

Styles IK, Feeney OM, Nguyen TH, Brundel DHS, Kang DW, Clift R, Mcintosh MP, Porter CJH (2019) Removal of interstitial hyaluronan with recombinant human hyaluronidase improves the systemic and lymphatic uptake of cetuximab in rats. J Control Release 315:85–96. https://doi.org/10.1016/j.jconrel.2019.10.040

Thao LQ, Byeon HJ, Lee C, Lee S, Lee ES, Choi YW, Choi H-G, Park E-S, Lee KC, Youn YS (2016) Doxorubicin-bound albumin nanoparticles containing a TRAIL protein for targeted treatment of colon cancer. Pharm Res 33:615–626. https://doi.org/10.1007/s11095-015-1814-z

Toole B (1973) Hyaluronate and hyaluronidase in morphogenesis and differentiation. Amer Jool 13:1061–1065. https://doi.org/10.1093/icb/13.4.106

Tran P, Lee S-E, Kim D-H, Pyo Y-C, Park J-S (2019) Recent advances of nanotechnology for the delivery of anticancer drugs for breast cancer treatment. J Pharm Invest 50:261–270. https://doi.org/10.1007/s40005-019-00459-7

Whatcott CJ, Han H, Posner RG, Hostetter G, Von Hoff DD (2011) Targeting the tumor microenvironment in cancer: why hyaluronidase deserves a second look. Cancer Discov 1:291–296. https://doi.org/10.1158/2159-8290.CD-11-0136

Youn YS, Bae YH (2018) Perspectives on the past, present, and future of cancer nanomedicine. Adv Drug Deliv Rev 130:3–11. https://doi.org/10.1016/j.addr.2018.05.008

Yuan B, Chen N, Zhu Q (2004) Emission and absorption properties of indocyanine green in Intralipid solution. J Biomed Opt 9:497–504. https://doi.org/10.1117/1.1695411